PNAS RESEARCH ARTICLE | MEDICAL SCIENCES

A TGF-β/KLF10 signaling axis regulates atrophy-associated genes to induce muscle wasting in pancreatic cancer

Aneesha Dasgupta[a,b,c,d,1,2], Daniel F. Gibbard[e,1], Rebecca E. Schmitt[a,b,c,d], Paige C. Arneson-Wissink[a,e], Alexandra M. Ducharme[a], Elizabeth S. Bruinsma[a], John R. Hawse[a,e], Aminah Jatoi[f], and Jason D. Doles[a,b,c,d,e,2]

Edited by Alfred Goldberg, Harvard Medical School, Boston, MA; received September 2, 2022; accepted June 14, 2023

Cancer cachexia, and its associated complications, represent a large and currently untreatable roadblock to effective cancer management. Many potential therapies have been proposed and tested—including appetite stimulants, targeted cytokine blockers, and nutritional supplementation—yet highly effective therapies are lacking. Innovative approaches to treating cancer cachexia are needed. Members of the Kruppel-like factor (KLF) family play wide-ranging and important roles in the development, maintenance, and metabolism of skeletal muscle. Within the KLF family, we identified KLF10 upregulation in a multitude of wasting contexts—including in pancreatic, lung, and colon cancer mouse models as well as in human patients. We subsequently interrogated loss-of-function of KLF10 as a potential strategy to mitigate cancer associated muscle wasting. In vivo studies leveraging orthotopic implantation of pancreas cancer cells into wild-type and KLF10 KO mice revealed significant preservation of lean mass and robust suppression of pro-atrophy muscle-specific ubiquitin ligases Trim63 and Fbxo32, as well as other factors implicated in atrophy, calcium signaling, and autophagy. Bioinformatics analyses identified Transforming growth factor beta (TGF-β), a known inducer of KLF10 and cachexia promoting factor, as a key upstream regulator of KLF10. We provide direct in vivo evidence that KLF10 KO mice are resistant to the atrophic effects of TGF-β. ChIP-based binding studies demonstrated direct binding to *Trim63*, a known wasting-associated atrogene. Taken together, we report a critical role for the TGF-β/KLF10 axis in the etiology of pancreatic cancer–associated muscle wasting and highlight the utility of targeting KLF10 as a strategy to prevent muscle wasting and limit cancer-associated cachexia.

muscle wasting | cachexia | pancreatic cancer | KLF10 | TGF-β

Significance

Skeletal muscle wasting is a serious cancer comorbidity that directly impacts therapeutic response, surgical prognosis, quality of life, and overall survival. Effective treatments targeting cancer-associated muscle wasting are limited. TGF-β signaling is well established as a driver of cancer-associated muscle wasting, but precise mechanisms of action remain unclear. We present evidence that the TGF-β target gene KLF10 is a key mediator of pancreatic cancer–associated muscle wasting. We further demonstrate that KLF10 can be targeted to prevent muscle wasting. Ultimately, this work provides key evidence in support of targeting the TGF-β/KLF10 signaling axis in wasting cancer patients to improve clinical outcomes.

Cancer cachexia is a syndrome characterized by muscle mass loss—that cannot be reversed with nutritive support—and is associated with reduced chemotherapeutic efficacy, poor prognosis, and diminished quality of life (1, 2). The prevalence of cachexia varies across cancer types, with the highest incidence observed in pancreatic ductal adenocarcinoma (PDAC) (3). Given the poor prognosis for patients presenting with or acquiring muscle loss, effective therapeutic interventions are needed.

Murine and cell-based models are frequently used to probe the molecular underpinnings of cachexia; indeed, foundational discoveries with respect to wasting-associated inflammation and cytokine signaling (i.e., interleukin, tumor necrosis factor, and TGF-β signaling) were made using mouse models. While neutralizing some of these cytokines or preventing signaling at the receptor level can alleviate cachectic burden in mice (4, 5), clinical trials of such treatments have had far less success (6, 7). This discovery–translational–clinical disconnect points to a need to develop a more nuanced understanding of these critical signaling pathways in cancer cachexia.

TGF-β superfamily members have been extensively researched in the context of cachexia. Activins A and B, Myostatin, and TGF-β are potent negative regulators of muscle size; indeed several studies show higher levels of these factors in cachectic mice and further indicate that blockade of several individual TGF-β superfamily members can abrogate muscle wasting in multiple mouse models of cancer (4, 7). More effective than neutralizing any one of these factors is targeting all of them, as evidenced in a recent study from Chen et al. where combined inhibition of Myostatin and Activin receptors resulted in prevention of cancer-associated wasting to a degree not achieved by targeting either individually (5). This study further demonstrated the efficacy of a pan-TGF-β targeting approach with respect to muscle hypertrophy in normal, disease-free mice. In this context, they observed substantially higher muscle weights by antagonizing both receptors instead of either receptor individually. These data suggest that common TGF-β superfamily member signaling effectors may be useful targets for modulating muscle size in a therapeutic context.

Author contributions: A.D., D.F.G., A.J., and J.D.D. designed research; A.D., D.F.G., R.E.S., P.C.A.-W., and A.M.D. performed research; E.S.B., J.R.H., and A.J. contributed new reagents/analytic tools; A.D., D.F.G., P.C.A.-W., A.M.D., A.J., and J.D.D. analyzed data; and A.D., D.F.G., R.E.S., and J.D.D. wrote the paper.

The authors declare no competing interest.

This article is a PNAS Direct Submission.

Copyright © 2023 the Author(s). Published by PNAS. This article is distributed under Creative Commons Attribution-NonCommercial-NoDerivatives License 4.0 (CC BY-NC-ND).

[1]A.D. and D.F.G. contributed equally to this work.

[2]To whom correspondence may be addressed. Email: aneedasg@iu.edu or jadoles@iu.edu.

This article contains supporting information online at https://www.pnas.org/lookup/suppl/doi:10.1073/pnas.2215095120/-/DCSupplemental.

Published August 16, 2023.

Several members of the Kruppel-like factor (KLF) family are reported to be both induced by TGF-β superfamily signaling and found to play important roles in many aspects of muscle biology and development, including proliferation and differentiation of satellite cells, lipid and amino acid metabolism, and hypertrophy/atrophy responses (8). KLF15 is a known regulator of nutrient flux in muscle cells, where it is required for effective lipid metabolism (9). KLF15 can also promote muscle atrophy in multiple contexts, including hyperglycemia-associated muscle mass loss and dexamethasone treatment, and is known to associate with Foxo1 and lead to increases in the atrogenes *Fbxo32* and *Trim63* (10, 11). KLF10 or TIEG1 (TGFβ-inducible early gene 1) was discovered as a downstream target of TGF-β signaling (12). KLF10 is regulated by the SMAD-2/3/4 complex and can reciprocally induce the expression of SMAD-2 (13). Moreover, KLF10 binds to the proximal promoter and represses the expression of SMAD-7, which is an inhibitory regulator of TGF-β signaling, thereby reinforcing the importance of TGF-β signaling cascade. KLF10 knockout (KO) mice display several phenotypic changes in female mice, including muscle hypertrophy, altered fiber area distribution, an increase in type II muscle fibers and fragile bones (14). Despite KLF10 being a major player in the TGF-β signaling, little is known about 1) the role of KLF10 in directly regulating muscle hypertrophy/atrophy and 2) the precise mechanisms responsible for the observed skeletal muscle phenotypes (15).

In vitro data from several groups suggest that KLF10 overexpression can inhibit proper muscle function by preventing differentiation of C2C12 cells and transcriptionally repressing FGFR1 expression, critical for proper proliferation and differentiation of myoblasts (16, 17). Thus, KLF10 appears to not only be involved in controlling muscle size, but also in the anabolic process of muscle repair and regeneration. In this study, we sought to explore the role of KLF10 in the etiology of cancer cachexia.

Results

KLF10 Is Up-Regulated in Cachectic Skeletal Muscle and in Response to Wasting Stimuli. There are 16 known KLF family members (18). Most are implicated in various aspects of muscle development including proliferation, differentiation, metabolism, repair, and atrophy (Fig. 1*A*) (8–11, 16, 17, 19–21). We reanalyzed data from several published reports and noted significant increases in KLF9, KLF10 and KLF15 in wasting skeletal muscle from KPC (22, 23) and Lewis Lung Carcinoma (LLC) (24, 25) cancer cachexia models (Fig. 1 *B* and *C* and *SI Appendix*, Fig. S1 *A* and *B*). In a human cancer cachexia dataset, KLF10 was the only KLF family member (out of KLF9, 10 and 15) up-regulated in PDAC patient muscle (Fig. 1*D*) (26). In support of these retrospective observations, we queried an in vitro model of muscle wasting, whereby cancer-conditioned medium (CM) was added to C2C12 myotubes to determine if atrophy stimuli directly induced expression of KLF10. In accordance with prior studies, we observed myotube thinning (atrophy) with the addition of T4-KPC CM to C2C12 myotubes (Fig. 1*E*). qRT-PCR analysis revealed significant KLF10 upregulation coincident with expected increases in the muscle-specific ubiquitin ligases *Trim63* and *Fbxo32* and other atrophy-associated transcripts including *Foxo1 and Foxo3* (Fig. 1 *E* and *F*).

KLF10 Loss-of-Function Prevents Cancer-Associated Skeletal Muscle Wasting. We orthotopically implanted T4-KPC cells into KLF10 wild-type (WT) and KLF10 KO mice to assess the role of KLF10 in mediating muscle wasting in tumor-bearing mice (Fig. 2*A*). KLF10 loss-of-function/downregulation in skeletal muscle was confirmed by qRT-PCR (Fig. 2*B*). No significant differences in longitudinal tumor volume, body weight, and fat mass were observed between WT and KO cohorts (Fig. 2 *C*–*E*). We did, however, observe longitudinal preservation of muscle mass in KO mice (Fig. 2*F*). Moreover, expression of atrophy markers *Trim63* (MuRF1) and *Fbxo32* (Atrogin-1) were significantly decreased in the KLF10 KO muscles (Fig. 2*G*). This mass preservation and diminished atrogene expression was associated with increased myofiber cross-sectional area (CSA) and minimum feret diameter in KO muscle (Fig. 2 *H* and *I*). We also observed that CSA and minimum feret diameters of control (nontumor bearing) KO muscles were smaller than their WT counterparts (*SI Appendix*, Fig. S2 *A* and *B*). Moreover, myofiber type analysis did not reveal any significant differences in myosin heavy chain isoform expression (and thus myofiber "types") between the WT and KO tumor-bearing muscles (*SI Appendix*, Fig. S2*C*).

Next, we isolated satellite cells (SCs) from KLF10 WT and KO skeletal muscle and differentiated SCs to form myotubes. Upon addition of cancer CM, we observed a decrease in myotube width in WT myotubes but not in KO myotubes (Fig. 2 *J* and *K*). We also observed an increase in atrophy markers in WT SCs but not in KO SCs upon CM treatment (Fig. 2*L*). Together, these data indicate that KLF10 loss-of-function limits activation of the muscle/myotube atrophy program in vitro and prevents cancer-associated skeletal muscle loss in vivo.

TGF-β Is a Critical Upstream Regulator of KLF10. We next performed RNA-sequencing analyses on muscle samples from tumor-bearing mice (WT and KO) to better pinpoint the molecular mechanisms behind muscle mass preservation in the absence of KLF10 (27). Gene expression–based principal component analysis demonstrated distinct clustering of WT and KO muscle samples from tumor-bearing mice (Fig. 3*A*). Of note, 267 genes were significantly altered between the WT and KO samples utilizing a threshold of Log fold change >1 and P value <0.05 (Fig. 3*B*). Of the 267 differentially expressed genes (DEGs), we observed a decrease in expression of transcripts associated with cancer cachexia including established atrophy markers such as *Foxo1*, *Foxo3*, *UCPs*, *Zip14*, as well as transcripts involved in calcium signaling and autophagy (Fig. 3 *C* and *D*). While variable, immunoblotting of phosphorylated FoxO1 and AKT did not reveal significantly consistent differences in KLF10 KO versus WT muscle lysates (*SI Appendix*, Fig. S3 *A* and *B*) suggesting that muscle preserving effects of KLF10 loss may not be working through modulation of AKT signaling. Network mapping revealed TGF-β to be a key potential upstream regulator of KLF10 (Fig. 3*E*).

TGF-β Family Members Are Increased in Cachexia and Can Induce KLF10. Together considering 1) TGF-β upstream regulator prediction, 2) the known link between KLF10 and TGF-β, and 3) the prominent role of TGF-β in cancer cachexia, we next sought to assess levels of individual TGF-β family members in varied atrophy settings. In vitro, we added serum free DMEM to HPNE (control CM) and T4 KPC (cancer CM) cells for 24 h at 37°. Control DMEM without cells was also kept at 37° and used as an additional experimental control. CM was recovered and TGF-β isoform abundance quantified. We found that TGF-β1 was significantly up-regulated in KPC CM compared to DMEM and HPNE media (Fig. 4*A*). TGF-β2 and TGF-β3 were also significantly up-regulated in the KPC CM as compared to DMEM. We next performed a similar analysis using serum collected from tumor-bearing mice and observed that TGF-β1-3

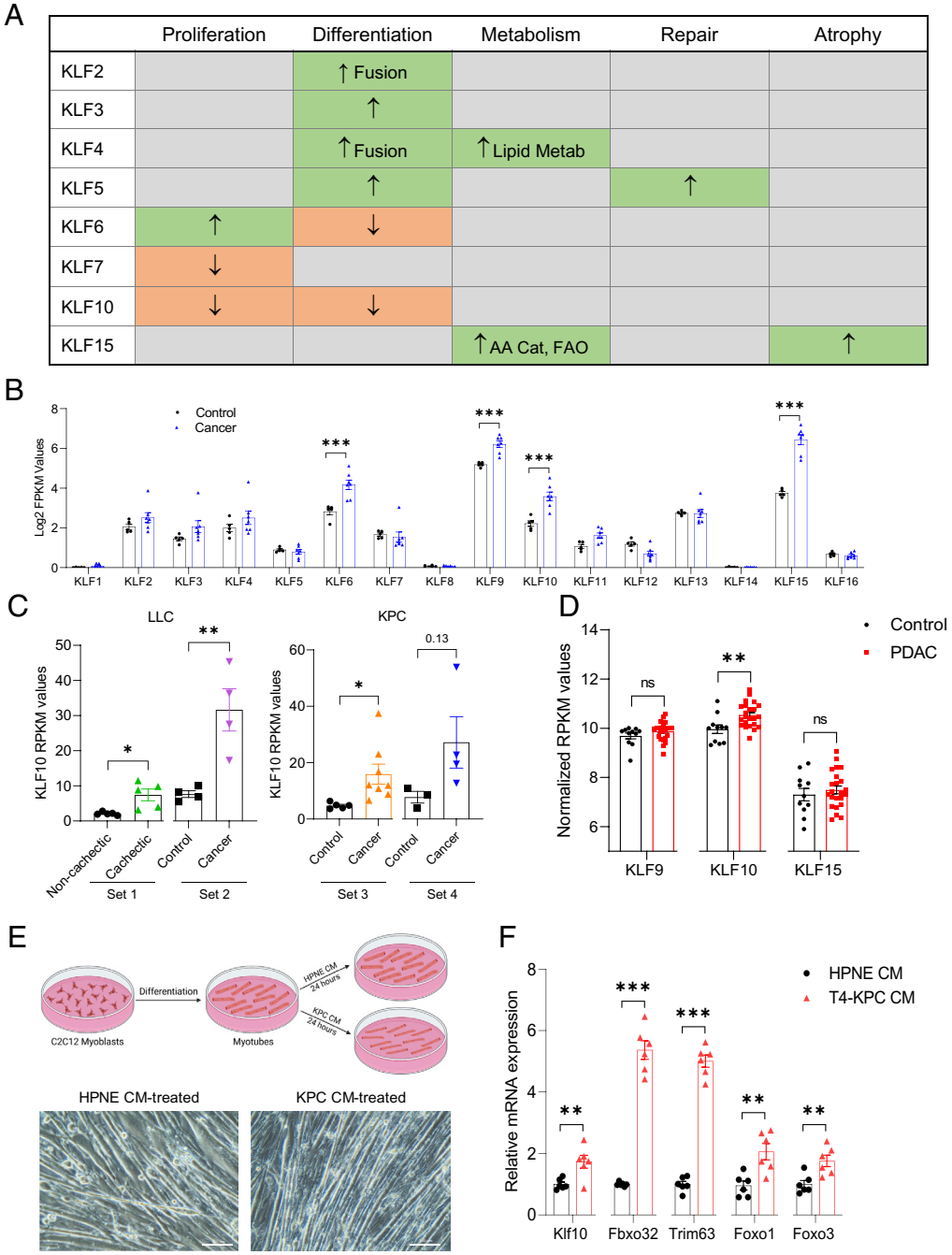

Fig. 1. KLF10 is up-regulated and associated with cancer cachexia. (*A*) Visual representation of reported roles of selected KLF family members in skeletal muscle. (*B*) Expression levels of KLF family members in muscles from pancreatic cancer tumor–bearing mice. n = 5 control, 7 tumor-bearing. (*C*) KLF10 expression levels between control and cachectic groups in four publicly available KPC and LLC muscle RNA-sequencing data sets. Set 1 – n = 5 each; Set 2 – n = 4 each; Set 3 – n = 5 control, 8 tumor-bearing; Set 4 – n = 3 control, 4 tumor-bearing. (GSE107470, PRJNA604626, PRJNA773714, and GSE123310) (D) Gene expression levels of identified KLF family members in a human muscle PDAC RNA-seq set. n = 11 control, 23 cachectic. (GSE133979) (*E*) Schematic and representative images of the treatment regimen for in vitro assessment of atrophy upon CM exposure. (Scale bar, 100 μm.) (*F*) Atrophy-related transcripts assessed by qRT-PCR of the myotubes shown in *E*. n = 6 each. Data shown are mean ± SEM and is compared using two-way ANOVA (*B*) with Bonferroni's post hoc correction, Student's unpaired *t* tests (*C*, *D*, and *F*). ns = nonsignificant, **P* < 0.05; ***P* < 0.01; ****P* < 0.001.

were all significantly increased in the serum of KPC-bearing mice as compared to control mice (Fig. 4*B*). Finally, serum analysis of cachectic patient serum revealed increased levels of TGF-β2 (Fig. 4*C*).

In order to investigate if TGF-β family members could directly induce the expression of KLF10, we treated C2C12 myotubes with TGF-β1 for 24 h and observed a significant induction in KLF10 mRNA expression (Fig. 4*D*). Next, we injected TGF-β1 (10 μg/mL) for 3 consecutive days in the gastrocnemius of WT and KO mice and subsequently queried atrogene expression. Five days postinjection, we observed significant increases in the expression of *Trim63* and *Fbxo32* in the TGF-β-treated WT mouse muscles but not in the KO mouse muscles (Fig. 4*E*). These data indicate that TGF-β-induced increase in atrophy gene expression requires KLF10.

KLF10 Binds to Atrophy Genes in the Presence of Wasting Stimuli. We next sought to investigate the mechanism by which KLF10 promotes muscle atrophy. Chromatin immunoprecipitation

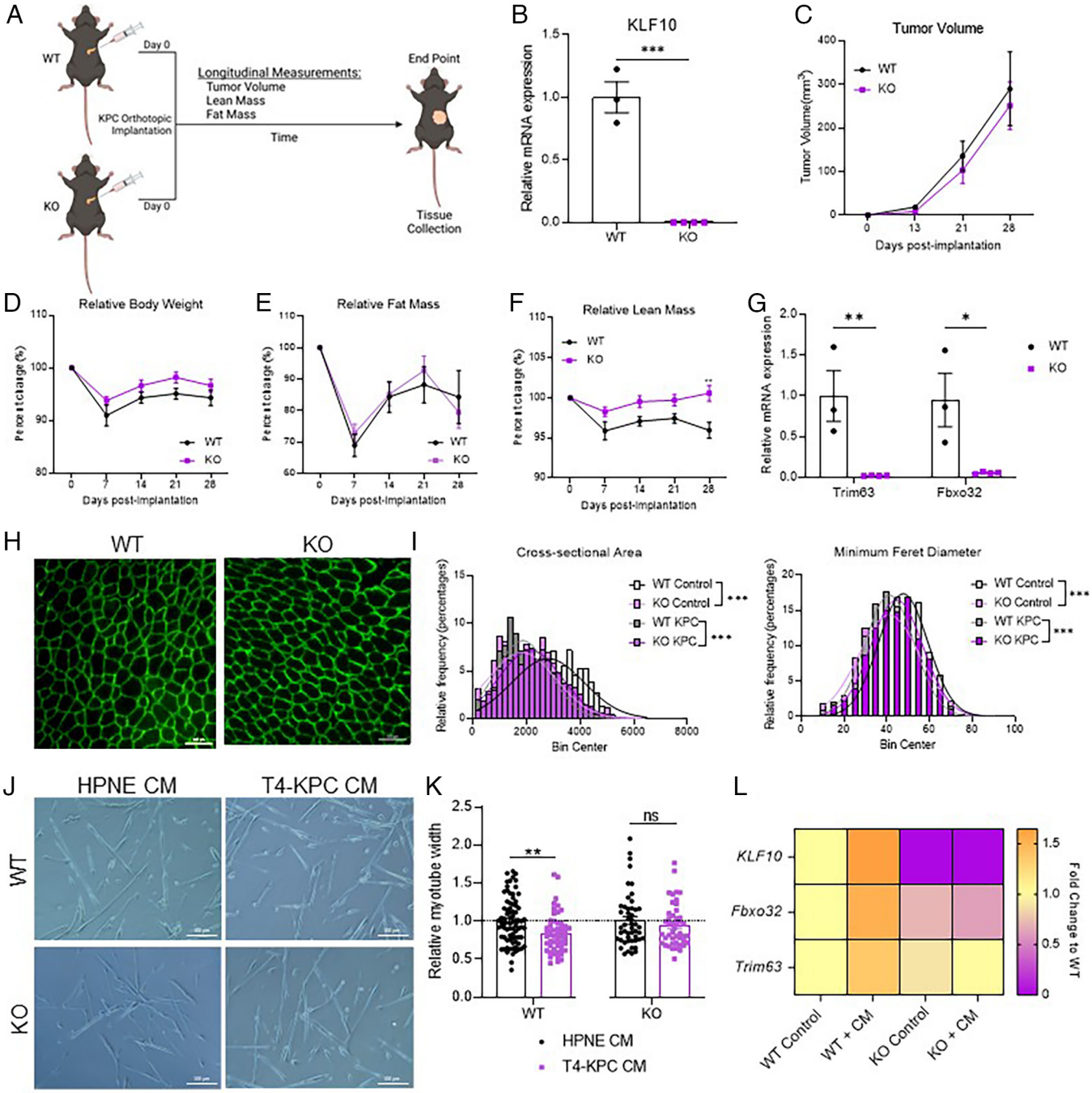

Fig. 2. KLF10 loss-of-function prevents muscle/myotube atrophy in vitro and in vivo. (*A*) Schematic detailing the tumor implantation procedure. (*B*) qRT-PCR confirming loss of KLF10 expression in KLF10$^{(-/-)}$ (KO) mice. n = 3 WT, 4 KO. (*C*) Tumor volume over the course of the study. (*D*) Changes in bodyweight, (*E*) lean mass, and (*F*) fat mass in tumor-bearing mice with respect to baseline measurements. (*G*) Quantification of atrophy-associated ubiquitin ligase Fbxo32 and Trim63 gene expression in the gastrocnemius muscle tissue of KO and WT mice at experimental end point. n = 3 WT, n = 4 KO. (*H*) Representative laminin immunostaining images to visualize muscle myofibers from KLF10 WT and KO mice at experimental end point. (Scale bar, 100 μm.) (*I*) Quantification of cross-sectional area and minimum feret diameter of muscle cross-sections from WT and KO mice. n = 3 WT/KO Control, n = 4 WT KPC, n = 3 KO KPC, n = 4 and n = 3 KO KPC mice for each group. (*J*) Representative images of WT and KO satellite cells treated with T4-KPC conditioned media for 48 h after differentiation. (Scale bar, 100 μm.) (*K*) Quantification of change in myotube widths in WT and KO with respect to control samples. n = 3 mice with six wells quantified each for each group, individual dots represent an individual myotube. (*L*) A heatmap of the expression of KLF10 and Ubiquitin ligases Fbxo32 and Trim63 in differentiated satellite cells upon treatment with conditioned media. Data shown are mean ± SEM and are compared using an unpaired *t* test (*B*, *G*, and *K*), Two-way ANOVA (*C*–*F*) with Bonferroni's Post hoc correction and comparison of best-fit values for gaussian nonlinear regression (*I*). ns = nonsignificant, *P < 0.05; **P < 0.01; ***P < 0.001.

(ChIP)-sequencing data of human cancer cell (https://www.omicsdi.org/dataset/geo/GSE90565) lines pointed to direct binding of KLF10 to several factors known to influence atrophy (Fig. 5*A*), including other KLF factors and Foxo1/Foxo3. To determine if KLF10 was directly binding to the promoter regions of atrophy genes in muscle cells (as opposed to tumor cells), we differentiated C2C12 cells in vitro before adding HPNE or T4 KPC conditioned media to stimulate myotube atrophy. Chromatin was collected for ChIP-qPCR analysis (see schematic in Fig. 5*B*), and qRT-PCR analysis performed targeting the muscle-specific ubiquitin ligases *Trim63* and *Fbxo32, Foxo1,* and *Foxo3*, and other KLF family members. We also queried *DMD* and *Col3a1* genes, which did

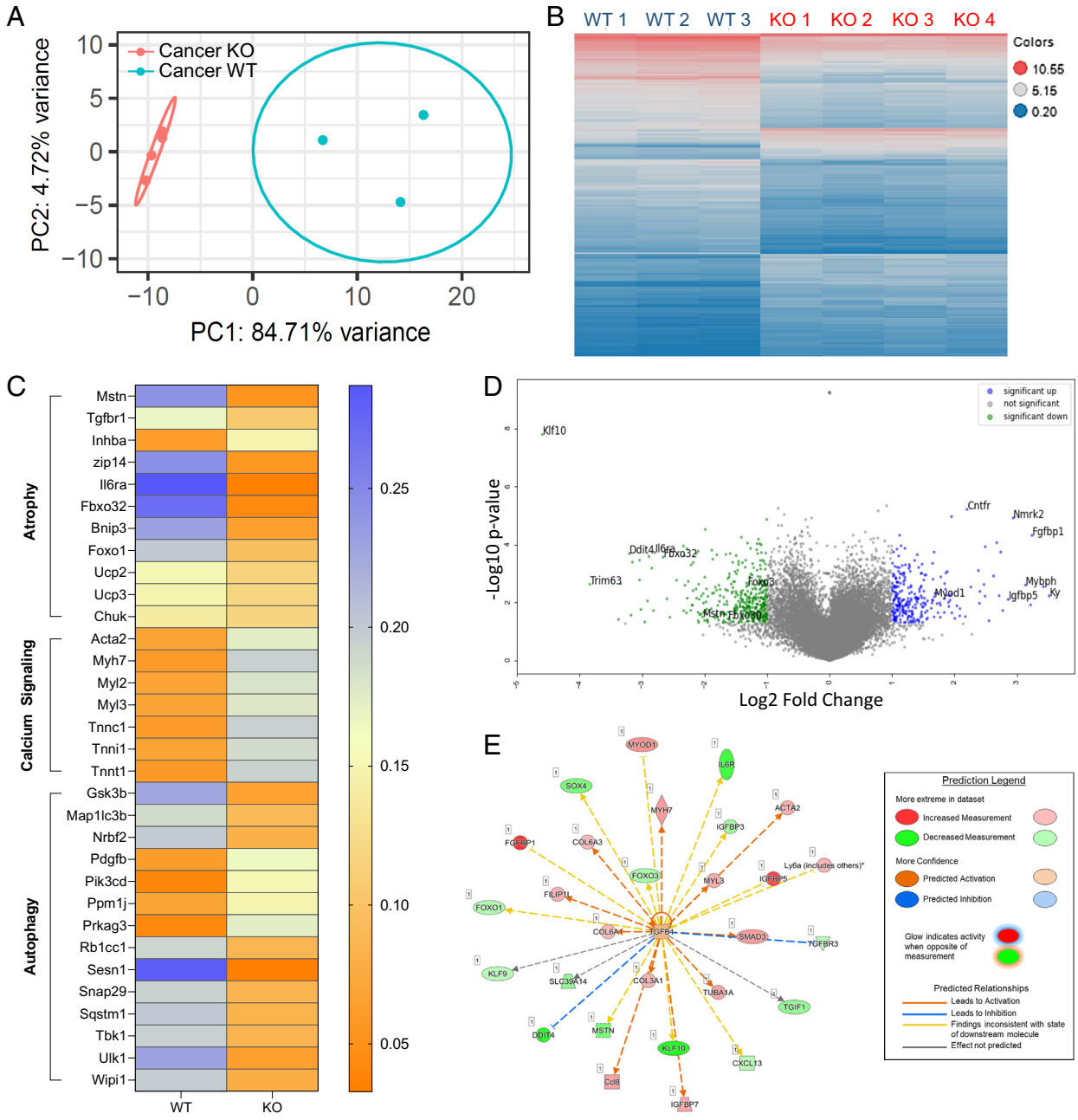

Fig. 3. RNA-sequencing analysis of skeletal muscle reveals distinct gene expression profiles in tumor-bearing KLF10 KO mice. (*A*) A principal component analysis (PCA) plot comparing tumor-bearing WT and KO mouse muscle. (*B*) A heatmap depicting differential expression of atrophy-related genes between KLF10 KO and WT tumor-bearing mice (*C*) A heatmap of DEGs between KLF10 KO and WT tumor-bearing mice. (*D*) A volcano plot highlighting selected DEGs between KLF10 WT and KLF10 KO cohorts. Green/left = significantly down in KLF10 KO; Blue/right = significantly up in KLF10 KO. (*E*) A network map highlighting TGF-β as a central regulator of many KLF10 KO DEGs. DEGs were shortlisted based on the threshold of log change = 1 and *P* value < 0.05.

not demonstrate any differences in gene expression between WT and KO muscles. We utilized primers complementary to the proximal and distal promoter regions (labeled as 1 or 2) of all queried genes. We found significantly increased occupancy of KLF10 at the distal promoter region of *Trim63* (Fig. 5*C*). Considered alongside observations of lower *Trim63* expression in tumor-bearing KLF10 KO mice, these data suggest a mechanism of action whereby KLF10 acts as a transcriptional activator to promote a muscle atrophy program.

KLF10 Inhibition Limits Skeletal Muscle Wasting in Tumor-Bearing Mice. To query the utility of KLF10 as a therapeutic target, we leveraged an adenoassociated virus (AAV; serotype 9)–based strategy to genetically silence KLF10 (shKLF10 AAV9) in tumor-bearing mice. AAV9 serotype has been demonstrated to target skeletal muscles upon systemic injection into mice. In our KPC tumor model, we injected GFP AAV9 (n = 7) and shKLF10 AAV9 (n = 7) 2 d prior to tumor cell implantation in male C57/BL6 mice (Fig. 6*A*). Thereafter, we performed weekly measurements of lean mass and tumor burden. While we did not observe a difference in overall survival between the control AAV9 and shKLF10 AAV9-injected tumor-bearing mice (Fig. 6*B*), we did observe lean mass preservation via longitudinal EchoMRI-based body composition analyses (Fig. 6*C*). Importantly, we did not observe differences in tumor weight at necropsy suggesting preservation of lean mass was independent of any potential intervention–associated decreases in tumor growth (Fig. 6*D*). At experimental endpoint, we observed increased *gastrocnemius* (GR), *tibialis anterior* (TA)

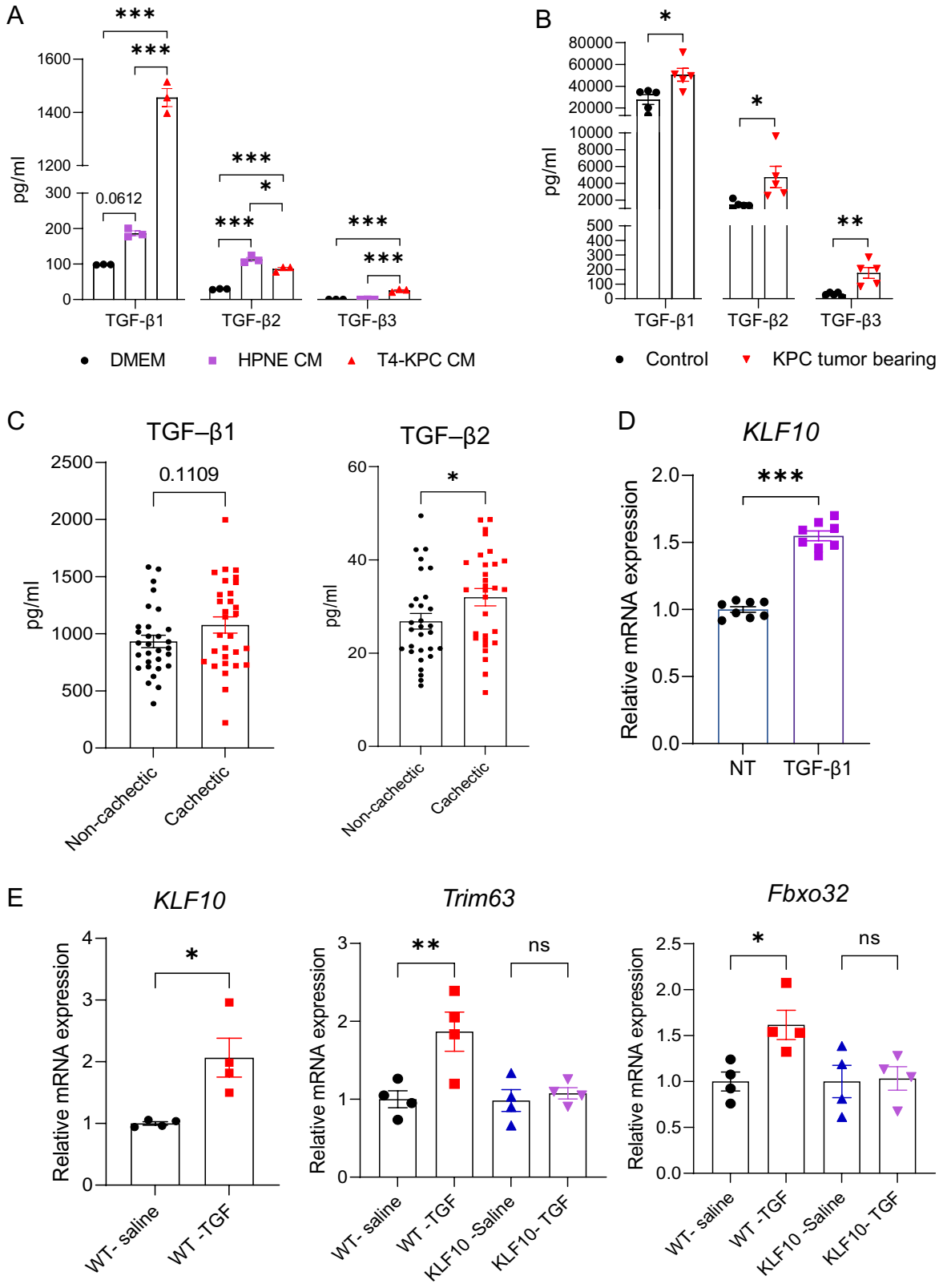

Fig. 4. KLF10 KO mice are resistant to the atrophic effect of TGF-β. (*A*) TGF-β protein levels in control media or conditioned media derived from T4-KPC cancer cells or HPNE control cells. n = 3 for each group. (*B*) Levels of TGF-β proteins in T4 KPC tumor-bearing mice n = 5 for each group. (*C*) TGF-β family protein levels in human cachectic patients n = 29 cachectic, 30 control. (*D*) KLF10 expression in C2C12 cells treated with TGF-β1 for 24 h. n = 8 for each group. (*E*) Gene expression quantification of *KLF10*, *Trim63*, and *Fbxo32*, in mice injected with TGF-β and saline. n = 4 for each group. Data shown are Mean ± SEM and are compared using one-way ANOVA (*A*) with Bonferroni's post hoc correction, Student's unpaired *t* test (*B*–*E*). ns = nonsignificant, **P* < 0.05; ***P* < 0.01; ****P* < 0.001.

and heart weights in shKLF10 AAV9 mice compared to controls (Fig. 6 *E*–*G*). Decreased KLF10 expression in shKLF10 AAV9 muscles (GR) was confirmed via qRT-PCR analysis (Fig. 6*H*). Similarly, we measured the expression of Trim63 and FbxO32 and observed reduced expression of both atrogenes, consistent with KLF10 KO experiments (Fig. 6*I*). CSA and minimum feret

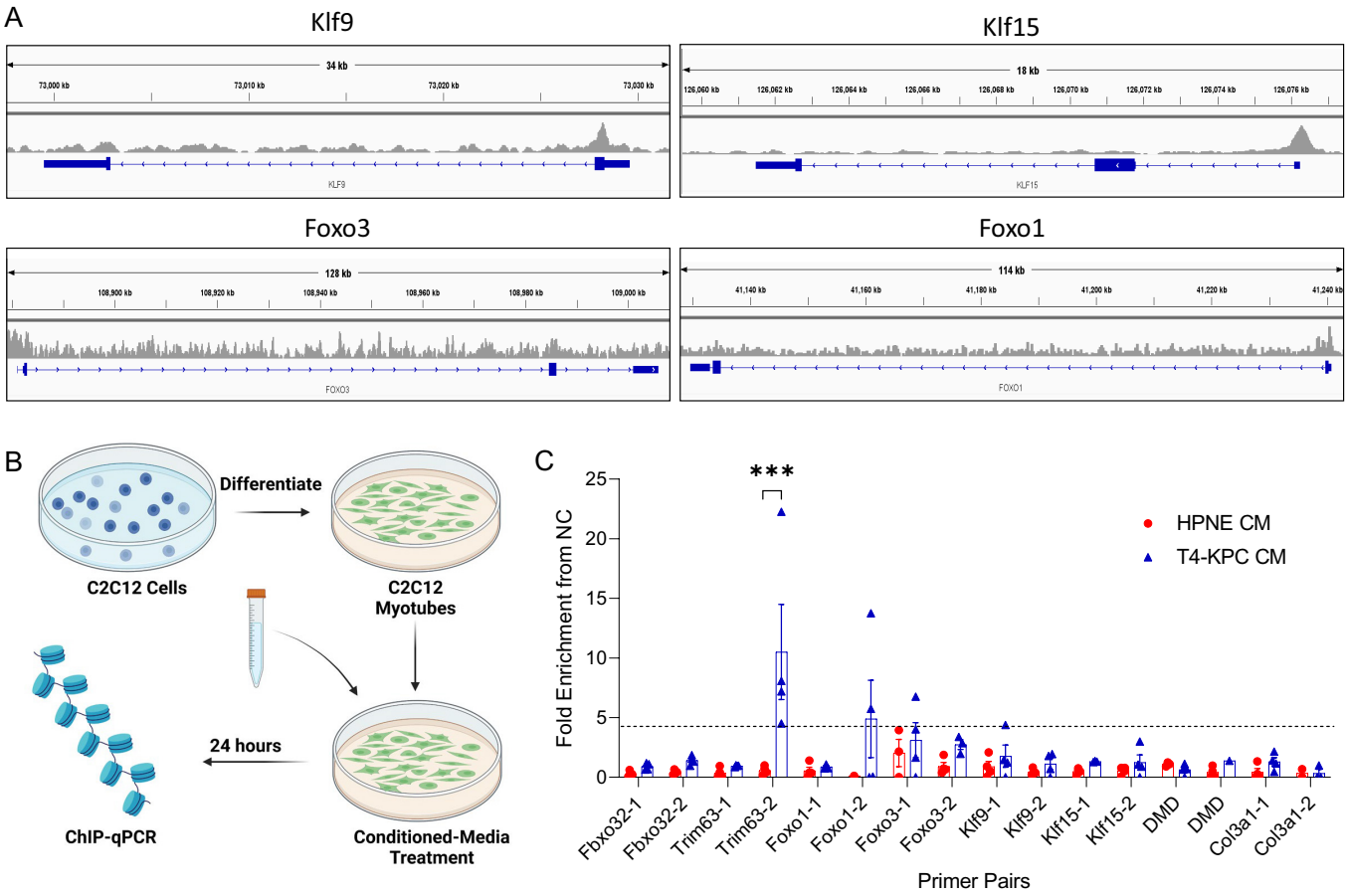

Fig. 5. ChIP analysis reveals potential targets of KLF10 (*A*) Integrated Genome Viewer (IGV) viewer tracks of Klf9, Klf15, Foxo1, and Foxo3 demonstrating KLF binding in human cancer cell sets. (*B*) Treatment schematic of cells undergoing ChIP-qPCR for a selected group of genes (*C*) Bar plot demonstrating enrichment of each primer set based on treatment with either T4 conditioned media or HPNE conditioned media. N = 4 replicates for each group. Data shown are Mean ± SEM and are compared using Student's unpaired *t* test (*C*). ns = nonsignificant, ***$P < 0.001$.

diameter measurements in muscle cross-sections further supported gross observations of muscle maintenance in shKLF10 AAV9 mice (Fig. 6 *J–L*). Myofiber MHC analysis did not reveal evidence of myofiber type switching between experimental groups (Fig. 6*M*). Taken together, our data show that targeting KLF10 in vivo can prevent tumor-induced skeletal muscle wasting and that KLF10 should be further interrogated as a potential therapeutic target for cancer-associated cachexia.

Discussion

TGF-β family members have been extensively investigated in the context of cancer cachexia—indeed changes in activins, TGF-β, and Bone morphogenetic proteins (BMPs) are linked to peripheral tissue wasting in diverse mouse models of cancer (28). Here, we studied the role of KLF10, a downstream effector of TGF-β, in the manifestation of muscle wasting/cachexia in a mouse model of pancreatic cancer. A major finding from our study was that KLF10 loss-of-function protected tumor-bearing mice from muscle loss. Gene expression studies aimed at better understanding the molecular underpinnings of this protection revealed a host of factors linked to cancer cachexia—including important wasting "atrogenes" like *Trim63* and *Fbxo32*, *Il6ra,* and *Mstn*, as well as genes (*Ky* and *Fgfbp1*) thought to be involved in protection of neuromuscular junctions, the stability of which have been implicated in cancer-associated muscle wasting and weakness (28, 29). These differentially expressed genes (DEGs) were shown by upstream regulator analysis to be under the control of TGF-β; highlighting KLF10's well-studied link to TGF-β as an inducible early gene. Noting this, our observation of muscle sparing effects in KLF10 KO mice is consistent with other reports where TGF-β function-blocking antibodies limit lean mass loss (4); however, we did not see an increase in survival as a result of KLF10 KO – an endpoint that would have to be investigated further given the relatively short tumor progression timeline associated with the KPC model. Our results further differ from other studies interrogating other TGF-β family members (i.e., activins and myostatin) in that, in our hands, KLF10 KO did not appear to cause muscle hypertrophy in the absence of stimuli (5).

Published studies revealed impaired myotube differentiation and altered myoblast proliferation upon KLF10 overexpression (17). Our gene expression analysis showed that tumor-bearing KLF10 KO mice had much higher levels of Myod1, a master regulator of muscle differentiation as well as promyogenic factors like Fgfbp1. To identify potential direct KLF10 targets, we performed ChIP-PCR of selected targets—including FoxO transcription factors, atrophy genes, and KLF family members. Ultimately, we found statistically significant KLF10 binding to Trim63, a critical atrophy factor. While intriguing, a limitation of our analysis was the biased selection of potential KLF10 binding candidates. A less-biased ChIP sequencing–based approach would permit a more robust/global survey of potential KLF10 targets in wasting muscle.

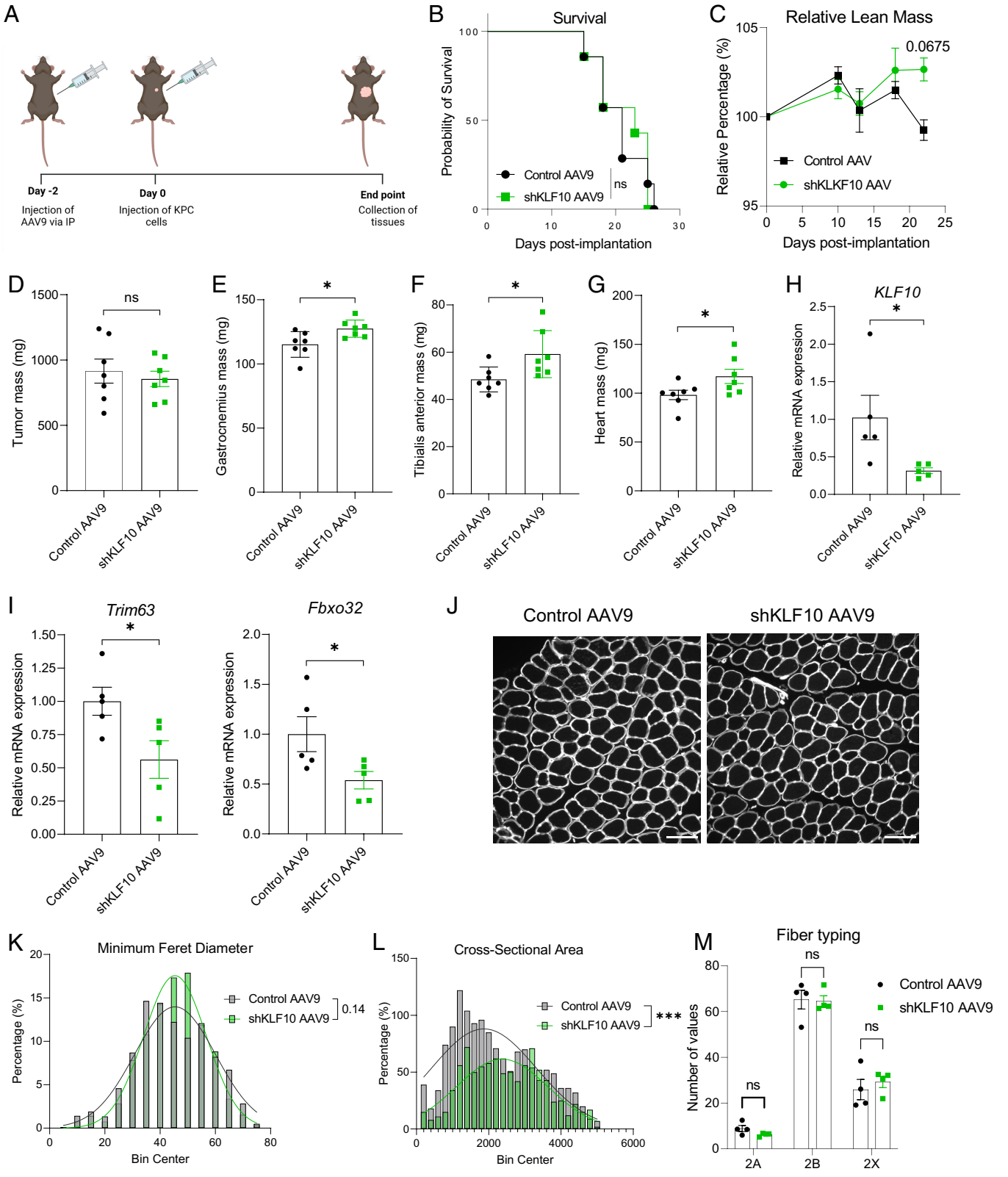

Fig. 6. Genetic inhibition of KLF10 prevents skeletal muscle loss associated with pancreatic cancer cachexia. (*A*) Schematic illustration of the experimental plan. Survival analysis (*B*), relative lean mass (*C*), postnecropsy tumor weight (*D*), Gastrocnemius weight (*E*), TA weight (*F*) and heart weight (*G*) of Control AAV9 (n = 7) and shKLF10 AAV9 (n = 7) injected mice. Relative mRNA expression of KLF10 (*H*), Trim63 (*I*) and FbxO32 in the gastrocnemius muscles of Control AAV9 (n = 5) and shKLF10 AAV9 (n = 5) injected mice. (*J*) Representative images of laminin-stained muscle sections of Control AAV9 and shKLF10 AAV9 at 20× magnification. (Scale bar, 100 μm.) (*K*–*L*) Minimum feret diameter and cross-sectional area measurements of cross-sections of Control AAV9 and shKLF10 AAV9 TA muscle. (*M*) Myofiber type quantification of both experimental cohorts. Data shown are mean ± SEM and are compared using Log-rank (Mantel-Cox) survival analysis (*B*), Student's unpaired *t* test (*D*–*I*), comparison of best-fit values for gaussian nonlinear regression (*K* and *L*), Two-way ANOVA with Bonferroni's correction (*C* and *M*). ns = nonsignificant, **P* < 0.05; ***P* < 0.01; ****P* < 0.001.

The role of KLF10 in resisting cachexia caused by other factors remains unknown. It should be noted that KLF10 upregulation is common among noncancerous atrophy models, such as chronic infection models and dexamethasone treatment (30, 31). Experiments testing resistance of KLF10 KO mice to atrophy stimuli outside of the TGF-β family would potentially reveal whether KLF10 exclusively mediates TGF-β-associated atrophy, or atrophy more broadly such as that associated with increased TNF-α or hindlimb unloading (32, 33). Because KLF10 expression appears to be more cell type and tissue restricted compared to TGF-β, targeting KLF10 may avoid a key pitfall associated with systemic TGF-β blockade—namely off-target effects. Thus, with respect to therapeutic development, KLF10 may represent a more attractive target than TGF-β ligands or associated receptors.

A limitation of utilizing KLF10 as a therapeutic target is that KLF10 is also known to function—in some contexts—as a tumor suppressor. Indeed, KLF10-deficient mice have an increased incidence of lung tumor formation, and KLF10 has a role in repressing SNAI2, a critical gene in the epithelial–mesenchymal transition (34, 35). Although we did not observe larger/more aggressive tumors or any difference in longevity in our implantation model, systemic inhibition of a potential tumor–suppressing factor such as KLF10 could present a substantial hurdle for the treatment of a cancer-associated cachexia. More detailed work needs to be performed to tease out the unique/differential pathways regulated by KLF10 in the PDAC tumor and skeletal muscle. In that regard, it is promising to note the absence of expression of muscle-specific E3 ligases in tumors—one of which seems to be a target of KLF10 in wasting muscle. Even so, muscle-directed strategies could permit KLF10-directed interventions even if potential targets are eventually revealed to be more extensive. Several recent advances in selective muscle targeting—including the use of skeletal muscle–related cell surface–specific proteins, antibody-drug conjugation techniques, nanoparticles, and extracellular vesicles (EVs)/exosomes— hold significant promise and may represent a means by which KLF10 inhibitors/degraders could be delivered to skeletal muscle to counteract cancer associated muscle wasting. Ultimately, this work provides key evidence in support of targeting TGF-β/KLF10-related signaling for the treatment of cancer cachexia and further implicates KLF10 as a key mediator of the catabolic muscle atrophy program.

Methods

Cell Culture and Reagents. Pancreatic cancer cell lines (T4-KPC cells) were derived from KPC mice as previously described (36) and were a kind gift from Gina Razidlo (Mayo Clinic, Rochester, MN). HPNE cells, a human pancreas cell line, were a gift from Martin Fernandez-Zapico (Mayo Clinic, Rochester, MN). All cell lines were cultured in Dulbecco's Modified Eagle Medium (DMEM; Gibco) with 10% Fetal bovine serum (FBS), 100 IU/mL penicillin, and 100 μg/mL streptomycin and incubated at 37 °C in a humidified incubator with 5% CO_2. C2C12 myoblasts were purchased from ATCC and cultured in DMEM with 10% FBS until confluent. After reaching confluency, the myoblasts were differentiated in DMEM with 2% horse serum (HS) and 1 μg/mL insulin for 72 h, as previously described (22).

Animal Studies. All animal experiments performed in this study were approved by the Mayo Clinic Institutional Animal Care and Use Committee (IACUC). C57BL/6 J mice were obtained from Jackson Laboratories. KLF10$^{(-/-)}$ mice were a generous gift from John Hawse (Mayo Clinic, Rochester, MN). Eight-week-old female mice were orthotopically implanted with 0.5 × 10^4 T4-KPC cells into the pancreas (22). Every week over the course of the experiment, the animals were weighed, had their tumors palpated, and measured with a caliper, and subjected to EchoMRI-based body composition analysis. Postnecropsy, tumor tissue and muscles were flash frozen in liquid nitrogen, formalin fixed, or incubated in 30% sucrose for further analysis. Mouse serum was also collected for downstream analysis.

AAV studies: Eight-week-old male C57BL/6 J were obtained from Jackson Laboratory. Mice were injected with 1 × 10^{11} vg of either GFP AAV9 (n = 7) or shKLF10 AAV9 (n = 7) via intraperitoneal injection. Two days postinjection, the mice were orthotopically implanted with 0.5 × 10^4 T4-KPC cells, and similar parameters were measured as above.

EchoMRI Imaging. An EchoMRI (magnetic resonance imaging) Body Composition Analyzer (Echo Medical Systems) was used for measuring longitudinal lean and fat mass as previously described (24). All body composition inferences/analyses were performed using the accompanying EchoMRI software.

Conditioned Media preparation. KPC or HPNE cell lines were cultured in DMEM with 10% FBS as previously described (37). Briefly, cells were seeded and allowed to reach 70% confluency. Next, cells were washed twice with 1× PBS and cultured in serum-free DMEM for 24 h. Media were collected and centrifuged at 3,000 rpm for 10 min, and the supernatant was collected in a fresh tube to be either used immediately or stored at −80 °C for future use. Equal number of cells was utilized to prepare batches of CM and reconstituted with 2% horse serum. C2C12 myotubes were incubated with CM for 24 h.

Isolation, Culture, and Differentiation of Muscle Satellite Cells. Muscle satellite cells were isolated as previously described (38)**.** Briefly, all hindlimb muscles were harvested, minced, and dissociated using 0.2% collagenase II (Gibco). A Satellite Cell Isolation Kit (Miltenyi) was used following the manufacturer's instructions to isolate satellite cells. Once isolated, satellite cells were grown in growth media containing DMEM/F12 plus 20% FBS, 10% HS, 1% chick embryo extract, 100 IU/mL penicillin, and 100 μg/mL streptomycin, 0.1% Amphotericin B (Corning), and 0.2% Fibroblast Growth Factor 2. Satellite cells were maintained at 37 °C and 5% oxygen. Myogenic differentiation was performed by seeding wells at 1,000 cells per square centimeter and given differentiation media containing DMEM/F12 with 2% HS and 100 IU/mL penicillin, and 100 μg/mL streptomycin. Micrograph pictures of differentiated satellite cells were taken at 20× in phase contrast. ImageJ (39) was used to quantity 5 measurements along the length of each myotube. These measurements were averaged, and five images were quantified per group.

RNA Isolation and qRT-PCR. Total RNA was extracted from cells or tissue lysates by using TRIzol reagent (Invitrogen) as previously described (22). RNA was purified using RNAeasy columns (Qiagen), as per the manufacturer's protocols. Purified RNA was either utilized for RNA-sequencing or for qRT-PCR. For qRT-PCR, the cDNA synthesis kit (Applied Biosystems) was utilized to obtain cDNA according to the manufacturer's protocol. qRT-PCR was performed using SYBR Green master mix (Biorad). *Tubulin* and *Gapdh* were used as internal controls. Relative gene expression analysis was performed by using the ΔΔCt method, as described previously (37).

RNA-Sequencing Analyses. RNA extracted from cells and tissues was submitted to the Mayo Clinic Medical Genome Facility where RNA quality was determined using the Fragment Analyzer from AATI. Library preparation, sequencing, and analyses were performed as described previously (24). Ingenuity Pathway Analysis (IPA), Python, and Tibco Spotfire were used to perform tertiary analysis. The accession number is PRJNA988245 on NCBI SRA (https://www.ncbi.nlm.nih.gov/sra).

Immunostaining. Murine muscle tissues were placed in a sucrose sink (30%) overnight prior to embedding and sectioning. These tissues were then frozen in OCT, and sections (8 to 10 μm) were cut and fixed in 4% paraformaldehyde (PFA) for 5 min at room temperature. Once fixed, tissues were incubated with anti-laminin (Sigma 4HB-2) as previously described (24). Alexa fluorescent conjugate 488 (Invitrogen) was used as the secondary antibody. Myofiber images were analyzed using MyoVision software (40) to determine cross-sectional area (CSA) and minimum feret diameter parameters. The software mapped and calculated the cross-sectional area of objects between the range of 150 and 5,000 μm^3.

Myofiber Analysis. After fixing with 4% PFA as mentioned above, TA sections were stained to assess the presence of different MHC isoforms, and thus myofiber types, as previously described (41). Briefly, sections were incubated with BA-D5 (type I myofibers, supernatant, 1:100, DSHB), SC-71 (type IIa myofibers, supernatant, 1:100, DSHB), BF-F3 (type IIb myofibers, concentrate, 1:100, DSHB), and laminin (1:250, Sigma) diluted in 1% Bovine Serum Albumin (BSA). Alexa Fluor secondary antibodies (Invitrogen) were diluted 1:250 in 1% BSA: anti-mouse IgG2b-405, anti-mouse IgG1-488, anti-mouse IgM-594, and anti-rabbit IgG-647. ImageJ (39) cell counter

was used to manually assess myofiber types for quantification. All TA sections were negative for type I myofibers and were therefore not included in the myofiber typing quantification graphs.

ChIP-PCR. ChIP was performed utilizing the Active Motif ChIP-IT express kit (catalog 53008), according to the manufacturer's protocols. Briefly, confluent C2C12 myoblasts were differentiated in 15-cm dishes and treated with either HPNE or T4 KPC conditioned media for 24 h. Cells were fixed with formalin at a final concentration of 1%, quenched with glycine, and lysed using the Active Motif lysis buffer kit. Samples were sonicated on ice using an Analis model CV18 20 KHz ultrasonic processor at 60% power for 7 pulses of 30 s, with 30 s of resting in between. The KLF10 antibody was kindly provided by Dr. John Hawse (Mayo Clinic, Minnesota). Samples were incubated on magnetic beads with rotation overnight with either the negative control (IgG) or KLF10 antibody. Decross-linking was done using the Active Motif decross-linking buffer at 65 °C for 2.5 h. DNA was cleaned up using phenol/chloroform extraction followed by ethanol precipitation before performing qRT-PCR. Primers were designed utilizing the NCBI primer design tool within 50 bp of KLF10-binding sites described in previous reports (34). We used two primer sets for each gene. For existing ChIP seq data, Mishra et al. performed ChIP-seq for KLF10 in A549 cells. All tracks are derived from the file GSE90565_A549_merged_KLF10 and visualized in IGV (34).

Immunoblotting. Immunoblotting of p-FoxO1, total FoxO1, p-AKT, and total AKT was performed as previously described (37). Briefly, gastrocnemius muscles were homogenized in RIPA lysis buffer. The lysates were centrifuged at 13,000 rpm for 5 min, after which the supernatant was collected. Protein content was quantified using Bradford reagent. Primary antibodies against phospho-FoxO1(Ser256), Total FoxO1, Phospho-AKT (Ser473) and Total AKT were purchased from Cell Signaling Technology and used for probing specific proteins. α-Tubulin (Sigma Aldrich) was utilized as loading control.

TGF-β Quantification. Quantification of TGF-β family member levels in patient serum, murine serum, and conditioned media was performed by Eve Technologies.

Patient Samples. Serum from cachectic and noncachectic pancreatic patients was analyzed for the levels of TGF-β family members. All patients provided written informed consent, and the study was approved by the Mayo Clinic IRB. Patients were characterized as cachectic or noncachectic based on weight loss. Cachectic criteria required a minimum of 10% body weight loss over a 3-mo window.

Data, Materials, and Software Availability. Sequencing data are available at NCBI SRA (https://www.ncbi.nlm.nih.gov/sra) using accession number PRJNA988245 (27).

ACKNOWLEDGMENTS. We wish to thank members of the Doles lab for helpful discussions and manuscript suggestions. We also thank the Mayo Clinic Medical Genome Facility and Mayo Clinic Microscopy and Cell Analysis Core for experimental and technical support. J.D.D. was supported by NIH/National Institute of Arthritis, Musculoskeletal and Skin Diseases (NIH/NIAMS) R00AR66696, Career Development Awards from the Mayo Clinic SPORE in Pancreatic Cancer (NIH/NCI P50CA102701) and the American Association for Cancer Research/Pancreatic Cancer Action Network, the Fraternal Order of Eagles, and the Mayo Clinic Center for Biomedical Discovery.

Author affiliations: [a]Department of Biochemistry and Molecular Biology, Mayo Clinic, Rochester, MN 55905; [b]Department of Anatomy, Cell Biology, and Physiology, Indiana University School of Medicine, Indianapolis, IN 46202; [c]Indiana Center for Musculoskeletal Health, Indianapolis, IN 46202; [d]Tumor Microenvironment & Metastasis Program, Indiana University Simon Comprehensive Cancer Center, Indianapolis, IN 46202; [e]Mayo Clinic Graduate School of Biomedical Sciences, Mayo Clinic, Rochester, MN 55905; and [f]Department of Oncology, Mayo Clinic, Rochester, MN 55905

1. W. D. Dewys *et al.*, Prognostic effect of weight loss prior to chemotherapy in cancer patients. Eastern Cooperative Oncology Group. *Am. J. Med.* **69**, 491–497 (1980).
2. J. Bachmann *et al.*, Cachexia worsens prognosis in patients with resectable pancreatic cancer. *J. Gastrointest. Surg.* **12**, 1193–1201 (2008).
3. V. E. Baracos, L. Martin, M. Korc, D. C. Guttridge, K. C. H. Fearon, Cancer-associated cachexia. *Nat. Rev. Dis. Primers* **4**, 17105 (2018).
4. S. H. Greco *et al.*, TGF-beta blockade reduces mortality and metabolic changes in a validated murine model of pancreatic cancer cachexia. *PLoS One* **10**, e0132786 (2015).
5. J. L. Chen *et al.*, Specific targeting of TGF-beta family ligands demonstrates distinct roles in the regulation of muscle mass in health and disease. *Proc. Natl. Acad. Sci. U.S.A.* **114**, E5266–E5275 (2017).
6. I. Gueta, A. Altman, Y. Shoenfeld, The effect of blocking TNF-alpha in patients with cancer-related cachexia and anorexia. *Harefuah* **149**, 512–514, 551, 550 (2010).
7. T. Golan *et al.*, LY2495655, an antimyostatin antibody, in pancreatic cancer: A randomized, phase 2 trial. *J. Cachexia Sarcopenia Muscle* **9**, 871–879 (2018).
8. Y. Oishi, I. Manabe, Kruppel-like factors in metabolic homeostasis and cardiometabolic disease. *Front Cardiovasc. Med.* **5**, 69 (2018).
9. L. Fan *et al.*, Muscle Kruppel-like factor 15 regulates lipid flux and systemic metabolic homeostasis. *J. Clin. Invest.* **131**, e139496 (2021).
10. N. Shimizu *et al.*, Crosstalk between glucocorticoid receptor and nutritional sensor mTOR in skeletal muscle. *Cell Metab.* **13**, 170–182 (2011).
11. Y. Hirata *et al.*, Hyperglycemia induces skeletal muscle atrophy via a WWP1/KLF15 axis. *JCI Insight* **4**, e124952 (2019).
12. M. Subramaniam *et al.*, Identification of a novel TGF-beta-regulated gene encoding a putative zinc finger protein in human osteoblasts. *Nucleic Acids Res.* **23**, 4907–4912 (1995).
13. S. A. Johnsen, M. Subramaniam, T. Katagiri, R. Janknecht, T. C. Spelsberg, Transcriptional regulation of Smad2 is required for enhancement of TGFbeta/Smad signaling by TGFbeta inducible early gene. *J. Cell Biochem.* **87**, 233–241 (2002).
14. M. Kammoun *et al.*, Impact of TIEG1 deletion on the passive mechanical properties of fast and slow twitch skeletal muscles in female mice. *PLoS One* **11**, e0164566 (2016).
15. S. A. Johnsen, M. Subramaniam, R. Janknecht, T. C. Spelsberg, TGFbeta inducible early gene enhances TGFbeta/Smad-dependent transcriptional responses. *Oncogene* **21**, 5783–5790 (2002).
16. M. Miyake *et al.*, TIEG1 negatively controls the myoblast pool indispensable for fusion during myogenic differentiation of C2C12 cells. *J. Cell Physiol.* **226**, 1128–1136 (2011).
17. R. Parakati, J. X. DiMario, Repression of myoblast proliferation and fibroblast growth factor receptor 1 promoter activity by KLF10 protein. *J. Biol. Chem.* **288**, 13876–13884 (2013).
18. N. M. Pollak, M. Hoffman, I. J. Goldberg, K. Drosatos, Kruppel-like factors: Crippling and un-crippling metabolic pathways. *JACC Basic Transl. Sci.* **3**, 132–156 (2018).
19. M. G. Dionyssiou *et al.*, Kruppel-like factor 6 (KLF6) promotes cell proliferation in skeletal myoblasts in response to TGFbeta/Smad3 signaling. *Skelet Muscle* **3**, 7 (2013).
20. S. Hayashi, I. Manabe, Y. Suzuki, F. Relaix, Y. Oishi, Klf5 regulates muscle differentiation by directly targeting muscle-specific genes in cooperation with MyoD in mice. *Elife* **5**, e17462 (2016).
21. B. Spittau, K. Krieglstein, Klf10 and Klf11 as mediators of TGF-beta superfamily signaling. *Cell Tissue Res.* **347**, 65–72 (2012).
22. A. Dasgupta *et al.*, Anticachectic regulator analysis reveals Perp-dependent antitumorigenic properties of 3-methyladenine in pancreatic cancer. *JCI Insight* **7**, e153842 (2022).
23. J. E. Rupert *et al.*, Tumor-derived IL-6 and trans-signaling among tumor, fat, and muscle mediate pancreatic cancer cachexia. *J. Exp. Med.* **218**, e20190450 (2021).
24. P. C. Arneson-Wissink, A. M. Ducharme, J. D. Doles, A novel transplantable model of lung cancer-associated tissue loss and disrupted muscle regeneration. *Skelet Muscle* **10**, 6 (2020).
25. M. D. Goncalves *et al.*, Fenofibrate prevents skeletal muscle loss in mice with lung cancer. *Proc. Natl. Acad. Sci. U.S.A.* **115**, E743–E752 (2018).
26. A. Narasimhan *et al.*, Profiling of adipose and skeletal muscle in human pancreatic cancer cachexia reveals distinct gene profiles with convergent pathways. *Cancers (Basel)* **13**, 1975 (2021).
27. A. Dasgupta *et al.*, KLF10 WT and KO tumor-bearing mice muscles. Sequence Read Archive (SRA). https://www.ncbi.nlm.nih.gov/bioproject/PRJNA988245. Deposited 27 June 2023.
28. R. Sartori *et al.*, Perturbed BMP signaling and denervation promote muscle wasting in cancer cachexia. *Sci. Transl. Med.* **13**, eaay9592 (2021).
29. T. Taetzsch, M. J. Tenga, G. Valdez, Muscle fibers secrete FGFBP1 to slow degeneration of neuromuscular synapses during aging and progression of ALS. *J. Neurosci.* **37**, 70–82 (2017).
30. J. Wu *et al.*, Skeletal muscle antagonizes antiviral CD8(+) T cell exhaustion. *Sci. Adv.* **6**, eaba3458 (2020).
31. L. C. Hunt *et al.*, Integrated genomic and proteomic analyses identify stimulus-dependent molecular changes associated with distinct modes of skeletal muscle atrophy. *Cell Rep.* **37**, 109971 (2021).
32. M. B. Reid, Y. P. Li, Tumor necrosis factor-alpha and muscle wasting: A cellular perspective. *Respir. Res.* **2**, 269–272 (2001).
33. Y. Gao, Y. Arfat, H. Wang, N. Goswami, Muscle atrophy induced by mechanical unloading: Mechanisms and potential countermeasures. *Front Physiol.* **9**, 235 (2018).
34. V. K. Mishra *et al.*, Kruppel-like transcription factor KLF10 suppresses TGFbeta-induced epithelial-to-mesenchymal transition via a negative feedback mechanism. *Cancer Res.* **77**, 2387–2400 (2017).
35. A. Memon, W. K. Lee, KLF10 as a tumor suppressor gene and its TGF-beta signaling. *Cancers (Basel)* **10**, 161 (2018).
36. S. F. Boj *et al.*, Organoid models of human and mouse ductal pancreatic cancer. *Cell* **160**, 324–338 (2015).
37. A. Dasgupta *et al.*, SIRT1-NOX4 signaling axis regulates cancer cachexia. *J. Exp. Med.* **217**, e20190745 (2020).
38. J. Joseph, D. S. Cho, J. D. Doles, Metabolomic analyses reveal extensive progenitor cell deficiencies in a mouse model of duchenne muscular dystrophy. *Metabolites* **8**, 61 (2018).
39. C. A. Schneider, W. S. Rasband, K. W. Eliceiri, NIH Image to ImageJ: 25 years of image analysis. *Nat. Methods* **9**, 671–675 (2012).
40. Y. Wen *et al.*, MyoVision: Software for automated high-content analysis of skeletal muscle immunohistochemistry. *J. Appl. Physiol.* **1985**, 40–51 (2018).
41. R. E. Schmitt *et al.*, Muscle stem cells contribute to long-term tissue repletion following surgical sepsis. *J. Cachexia Sarcopenia Muscle* **14**, 1424–1440 (2023), 10.1002/jcsm.13214.